American Mineralogist, Volume 97, pages 1987–1997, 2012

On the origin of sellaite (MgF_2)-rich deposits in Mg-poor environments

KATHARINA PFAFF,* SEBASTIAN STAUDE, AND GREGOR MARKL

Fachbereich Geowissenschaften, Universität Tübingen, Wilhelmstrasse 56, 72074 Tübingen, Germany

ABSTRACT

Sellaite (MgF_2) forms from melts, fluids, and gases under variable temperature, pressure, f_{O2}, and fluid salinity conditions. It is typically associated with, but much rarer, than fluorite (CaF_2). The Clara mine near Oberwolfach (Schwarzwald, Germany) is an extensive hydrothermal vein-type deposit, where sellaite occurs in huge quantities (thousands of tons) in veins of mostly Jurassic/Cretaceous age. The sellaite mineralization, occurring in gneisses altered prior to and during sellaite mineralization, represents a stockwork-like network of veins and fissures, which is overlain and sealed by sediments, preventing the inflow of and fluid-mixing with sedimentary formation waters. The occurrence of sellaite is unique among the more than 1000 hydrothermal vein-type occurrences of the Schwarzwald ore district. The favored formation of sellaite compared to fluorite requires the initial Ca/Mg-ratio of the mineralizing fluid to be unusually low. These conditions are possible if fluids equilibrate with pre-altered rocks that lost some or much of their Ca during an earlier hydrothermal alteration event. Indeed, calculations demonstrate that rock-buffered fluids of pre-altered rocks (i.e., gneiss around the Clara mine altered during prior hydrothermal events) show significantly lower Ca/Mg-ratios than fluids equilibrated with unaltered gneisses, because Ca-phases (e.g., the anorthite component of plagioclase) are more prone to hydrothermal destruction. Due to the network-like structure of the sellaite-bearing portion of the Clara fluorite vein, the fluid is shielded from sedimentary formation water, resulting in fractionation processes of the repeatedly ascending mineralizing fluid. In addition, fluid cooling and formation of water-bearing phases like illite that consume fluids, favor sellaite, and later fluorite precipitation. The rarity of this combination of prerequisites explains the limited occurrence of sellaite in hydrothermal vein-type deposits.

Keywords: Sellaite, Clara mine, Schwarzwald, hydrothermal vein-type mineralization, fluid inclusion thermometry, fluid conditions

INTRODUCTION

Sellaite (MgF_2) is a rare mineral that occurs in variable geological settings. It can form under various different conditions (Table 1), ranging from magmatic [Oldoinyo Lengai, Tanzania; Nkombwa Hill, Zambia (Mitchell 1997; Zambezi et al. 1997; Keller and Krafft 1990)], sedimentary [New Brunswick, Canada (Grice et al. 2005)], metamorphic (Huanzala, Peru (Imai et al. 1985)], to hydrothermal environments [Suran, Russia (Ellmies et al. 1999)] and burning coal dumps [Chelyabinsk, Russia (Sokol et al. 2002)]. A locality with an unusually rich occurrence of sellaite is the Clara hydrothermal fluorite vein system in the Schwarzwald ore district, SW Germany (Maus 1977; Maus et al. 1979; Gerler 1983). This is an ideal locality for investigating the formation conditions of this unusual mineral because: (1) the Clara vein system is exposed as part of an operating mine, and (2) the Clara vein system is part of a well-investigated ore district (Schwarzwald ore district) where the geochemistry of host and possible source rocks (Hofmann and Köhler 1973; Matter et al. 1987; Schleicher 1994; Kalt et al. 2000), the formation age (e.g., Pfaff et al. 2009 and references therein), principal formation mechanisms (Schwinn et al. 2006; Baatartsogt et al. 2007; Staude et al. 2009, 2010a), ore-forming fluid conditions (Behr and Gerler 1987; Schwinn and Markl 2005; Markl et al. 2006a, 2006b; Staude et al. 2007, 2010b, 2011, 2012; Glodny and Grauert 2009; Pfaff et al. 2010), and structural control (Franzke et al. 2003; Staude et al. 2009) are well known.

In this study, we will explore the formation conditions of sellaite and investigate why the otherwise rare mineral sellaite occurs in large quantities in the Clara vein system within an elsewhere sellaite-free ore district.

GEOLOGY AND MINERALOGY OF THE CLARA VEIN SYSTEM

The complex vein system of the Clara mine was subdivided into numerous stages and sub-stages (Huck 1984). Stage 1 consists of a quartz-pyrite-dominated vein assemblage accompanied by intense host rock alteration and silification. In the following stage 2, the NW-SE-striking fluorite vein containing abundant sellaite formed. Stage 3 is represented by a parallel

---

* Present address: Department of Geology and Geological Engineering, Colorado School of Mines, 1516 Illinois Street, Golden, Colorado 80401, U.S.A. E-mail: kpfaff@mines.edu

0003-004X/12/1112–1987$05.00/DOI: http://dx.doi.org/10.2138/am.2012.4113

TABLE 1. Summary of sellaite-bearing localities

Environment	Host rock	Locality	Association	Formation temperature	Fluid conditions	Others	References
Hydrothermal	Metasedimentary gneiss	Clara mine, fluorite vein, Schwarzwald, SW Germany	Carbonates, fluorite, anhydrite, pyrite, quartz, barite	100–160 °C	Ca. 25wt% NaCl eq.	Mg leached from the pre-altered host rock	Maus (1977); Maus et al. (1979); Martin (1978); This work
		Fontsante, France	Fluorite				Mari (2002)
	Diabase, low-grade metamorphic schist, dolostone, marl	Suran, Russia	Fluorite	>250 °C	Highly saline (halite-daughter crystals in fluid inclusions)	Mg leached from the diabase	Ellmies et al. (1999)
	Dolomite	Kangding, Sichuan, China	Quartz, fluorite, native Au, bornite, galena, pyrite, bournonite, geocronite	220–280 °C	Fluid pressure: 30–60 MPa, pH weak alkaline	Sellaite formation due to fluid-rock interaction: decrease in pH and a_{H2S}	Li and Cai (1995)
	Pegmatite	Olary, SA, Australia	Fe-Mn phosphates, fluorite, thomsenolite/pachnolite, barite, calcite, Cu-sulfide	<250 °C	High f_{O_2}	Sellaite formation due to hydrothermal pegmatite alteration; Fluorite and Sellaite with upo to 2.1 wt% Al_2O_3	Lottermoser and Lu (1997)
Skarn	Meta-limestone	Huanzala, Peru	Calcite, quartz, phengite, dolomite, fluorite, talc, chlorite, gypsum, montmorillonite, kaolinite	330–200 °C	Ore-paragenesis in pyrite stability field regarding T, f_{O_2}, and pH	Formed during alteration of host rock during Cu-Ag-Sn mineralization	Imai et al. (1985)
	Meta-dolomite	Mt. Bischoff, Tasmania, Australia	Fluorite, quartz, dolomite, magnesite, illite, phlogopite, cassiterite, phengite, tourmaline, sphalerite, topaz	290–370 °C		Mg from dolomite-host rock	Wright and Kwak (1989); Halley and Walshe (1995); Walshe et al. (1996)
	Meta-dolomite	Fiano, Mt. Somma, Italy	Fluorite, fluoborite			Mg from sedimentary dolomite	Balassone et al. (2002)
Metamorphic	Magnesite	Brumado, Brazil	Quartz, magnesite, dolomite, dravite			Gem-quality sellaite crystals	Bodenlos (1954); Cassedanne and Resende (1983)
Carbonatite	Natrocarbonatite	Oldoinyo Lengai, Tanzania	Nyerereite, gregoryite, sylvite, fluorite, apatite, Fe-alabandite, witherite	491–544 °C of the melt	Formed from a melt	June 1988 eruption	Keller and Kraft (1990)
	Ankeritic dolomite carbonatite	Nkombwa Hill, Zambia	Dolomite, phlogopite, fluorite, apatite, isokite		Formed from a melt		Zambezi et al. (1997)
Sedimentary-diagenetic	Carnallitite	Hildesheim, Salzdetfurth, Germany	Carnallit, halite			Primary sellaite, formed during evaporation	Kühn (1951); Braitsch (1962)
	Dolomite	Bleicherode, Germany	Dolomite				Braitsch (1962)
	Halite	Kings County, New Brunswick, Canada	Halite, borate-minerals, anhydrite, fluorite, Fe-Cu-Ni-Zn-sulfides, calcite, magnesite, dolomite, hematite, organic material				Grice et al. (1996, 2005)
Secondary inclusions in diamond	Diamond	Unknown	Diamond, calcite, hematite, kaolinite, xenotime			Influene of kimberlite melt during sellaite formation	Harris (1969)
Burning coal dump	Coal, ankeritic marl	Chelyabinsk, Ural, Russia	Tridymite, anorthite, cordierite, mullite, periclase, fluorapatite, phlogopite, fluortopaz, fluorite			Sellaite formation due to reaction of gaseous fluorine with sedimentary carbonate	Sokol et al. (2002)

NW-SE-striking barite vein. Stage 4 consists of minor barite mineralization within older vein structures, and stage 5 is a W-E striking quartz-dominated vein (Diagonaltrum). Sellaite occurs in the stage 2 fluorite veins.

The Clara vein system is hosted by rocks of the Variscan crystalline basement and is covered by Lower Triassic sedimentary rocks (Gerler 1983; Huck 1984; Fig. 1a). The crystalline basement in the surrounding area consists of meta-sedimentary and meta-igneous rocks that are crosscut by NE-SW striking granitic dikes that are up to 30 m thick (Gerler 1983). The meta-sedimentary rocks are mainly heterogeneous gneisses with alternating biotite-rich and quartz- and plagioclase-rich layers

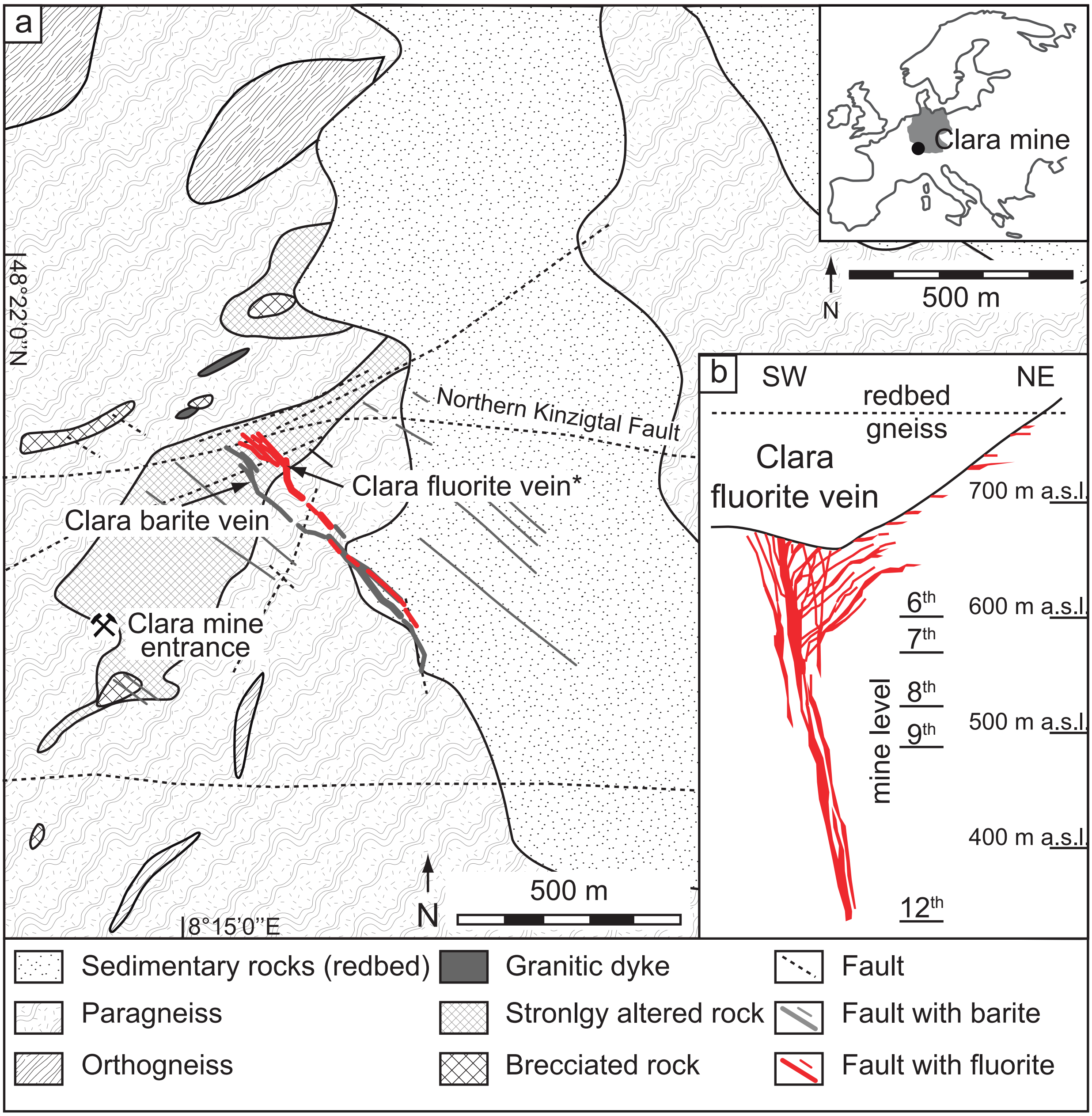

FIGURE 1. (**a**) Geological map of the area around the Clara vein system with the most important tectonic elements after Gerler (1983) and Huck (1984). Not shown are the stage 5 quartz-dominated veins of the "Diagonaltrum." * Note, the fluorite vein is predominantly exposed in the underground mine. (**b**) Cross section of the Clara fluorite vein (northern lens) after Huck (1984). (Color online.)

and migmatites. The primary rock-forming minerals are biotite, quartz, and plagioclase, with local enrichments of sillimanite (Gerler 1983). Orthoclase, garnet, and cordierite are important in some units; accessory minerals are apatite, zircon, titanite, and rutile. Lenses of hornblende-plagioclase-amphibolite (with local garnet) occur (Gerler 1983). The contact of the meta-sedimentary and meta-igneous rocks is sharp. The latter are homogeneous consisting of quartz, plagioclase, orthoclase, and biotite with accessory apatite, zircon, titanite, rutile, and sillimanite (Gerler 1983). The sedimentary cover discordantly overlies the basement rocks. The stratigraphically lowest unit is Upper Permian and Lower Triassic redbeds. The Lower Permian dolomite-dominated calcrete horizon that is found in many areas of the Schwarzwald district (Röper 1980) is lacking in the area around the Clara vein system. The stratigraphically lowest rocks of the redbed sequence consist of conglomerates containing clasts of quartz, feldspar, and basement rocks. These are overlain by sandstones and clays (Gerler 1983).

In some areas around the Clara vein system, an intense alteration occurred prior to fluorite stage 2 mineralization, which was accompanied by the formation of quartz-pyrite veins. These alteration zones strike NE-SW in most cases (Fig. 1a). In altered rocks, chlorite replaces biotite, sericite replaces plagioclase, and cordierite is replaced by pinite. Concomitantly to this alteration process, there was an intense silification together with hematite and pyrite growth (Huck 1984). During vein formation, irregular masses of cogenetic illite formed around the veins. The alteration of the sedimentary cover rocks is represented by intense silification (Gerler 1983; Maag 1987) and minor formation of feldspar and barite (Gerler 1983). The sellaite occurs not only in the fluorite veins but also in the previously altered paragneisses (Huck 1984).

OCCURRENCE OF SELLAITE IN THE CLARA VEIN SYSTEM AND SAMPLE DESCRIPTION

In the Clara mine, sellaite is exclusively present in the stage 2 fluorite vein. About 80% of the fluorite is in the 450 mm long northwestern part of the vein (Fig. 1a), which has been mined since 1975. The fluorite vein formed in several sub-phases: The first sub-phase 2.1 produced chalcedony and fluorite-filled breccias hosting rare Ag-Bi-bearing sulfosalts like matildite and berryite (Staude et al. 2010a). In stage 2.2, sellaite and fluorite-I

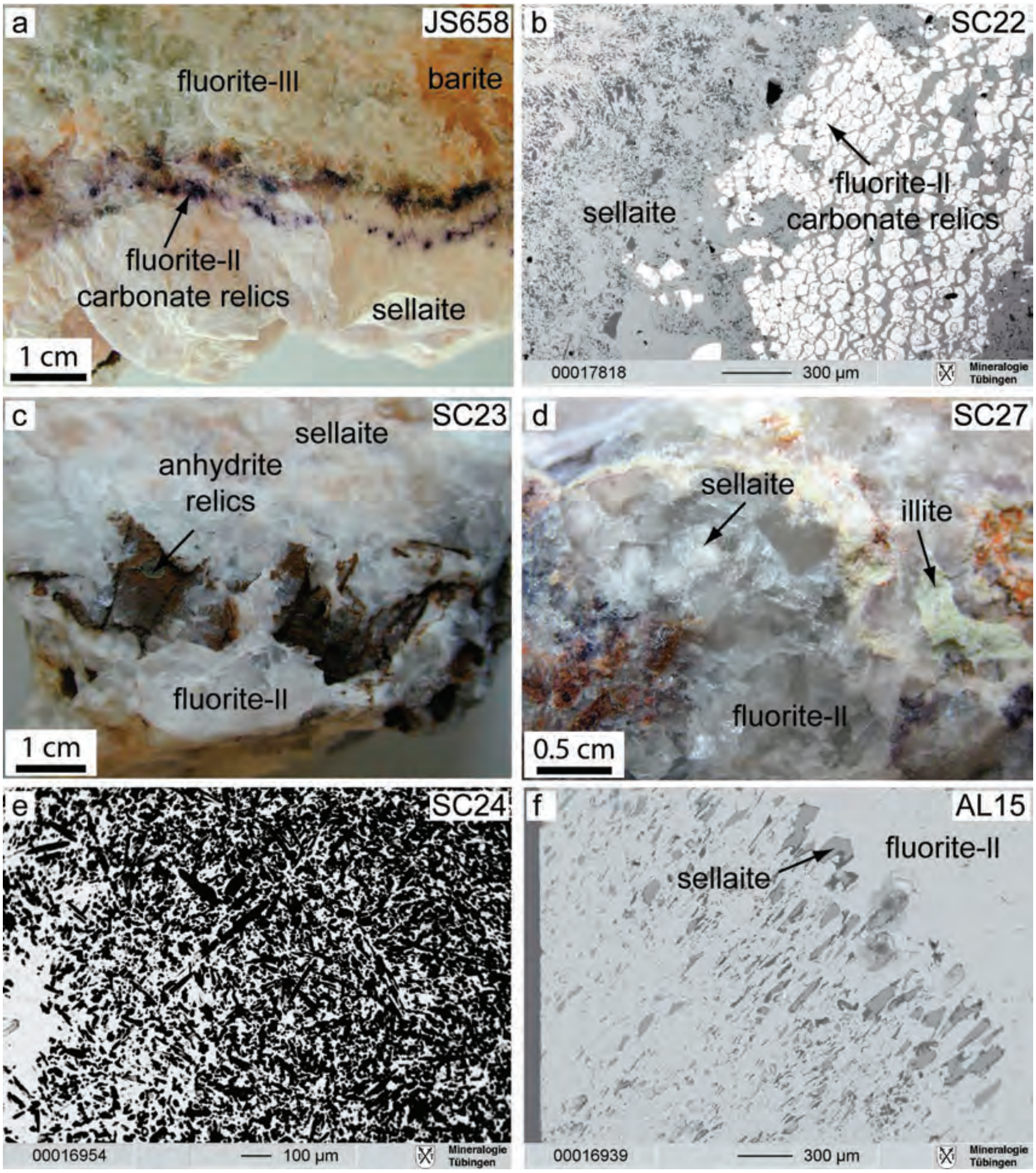

FIGURE 2. (**a**) Hand specimen of sellaite intergrown with relics of carbonates (that are now replaced by purple fluorite-II). (**b**) Hand specimen of sellaite overgrown by fluorite-II. Carbonate relics are replaced by fluorite. (**c**) Polished hand specimen of sellaite, partly replaced by fluorite-II. Carbonate relics are evident. (**d**) Hand specimen of sellaite-spherules in fluorite-II, which is intergrown with illite. (**e**) BSE-picture from the electron microprobe of former sellaite needles (black) intergrown with interstitial fluorite-I (gray). (**f**) BSE-picture from the electron microprobe of sellaite needles that are overgrown and partly replaced by fluorite-II. (Color online.)

are accompanied by ankerite, anhydrite, pyrite, and quartz. The last substage (stage 2.3) consists of quartz and fluorite, which replaced sellaite. Structurally, the sellaite-bearing stage 2.2 veins are unique among the more than 1000 known veins in the Schwarzwald ore district: they are bent by and split below the basement-cover unconformity (Huck 1984), forming a stockwork-like system (Fig. 1b), which was sealed from the surface by the overlying sediments but open to the influx of ascending fluid pulses. Irregular aggregates of illite are either enclosed in stage 2 fluorite, resulting in a milky haze of the fluorite, or form separate aggregates (Fig. 2d). Some minerals of the fluorite stage 2 could be dated: ferberite at 173 ± 2 Ma (U-Pb method; Pfaff et al. 2009), barite and fluorite at 130 ± 20 Ma (Rb-Sr method; Mertz et al. 1986), sericite at 143 ± 2 Ma (Rb-Sr method; Mertz 1987), and host-rock illite from the barite vein at 144 ± 5 Ma (Rb-Sr method; Mertz 1987).

Sellaite occurs as fibrous crystals that are up to 30 mm in length and up to 0.2 mm in diameter (Fig. 2). Typically, the crystals are arranged as radial aggregates that are up to 5 cm in diameter or more rarely as chaotic aggregates with interstitial fluorite-I (Fig. 2e). In most cases, sellaite grows around host rock fragments or relics of carbonate minerals (ankerite-relics can rarely be found and empty rhombohedral holes are interpreted as dissolved carbonates) and anhydrite (empty rectangular holes are interpreted as perimorphs after anhydrite; Figs. 2a–2c), which may be aligned in bands (Figs. 2a and 2b). A younger sellaite generation overgrows the first one and only rarely contains carbonate relics. Sellaite is overgrown and replaced by gray to greenish fluorite-II (Figs. 2b, 2d, and 2f), which frequently hosts irregular masses of illite (Fig. 2d). Commonly, fluorite in vugs are erroneously identified macroscopically as sellaite aggregates (Fig. 2e). The same generation of fluorite (fluorite-II) that replaces sellaite also replaces the carbonates and has a dark purple color (Fig. 2a). Sellaite—and fluorite that replaces sellaite (fluorite-II in Fig. 2)—is crosscut by a younger mineralization of bluish fluorite (fluorite-III) and barite. Rarely, the carbonates are also replaced by quartz and in one sample sellaite was replaced by secondary fluorite-IV and chisel-shaped barite (chisel-spar; Staude et al. 2011).

ANALYTICAL TECHNIQUES

Fluid inclusion analyses

Fluid inclusions were analyzed in doubly polished sections of sellaite and fluorite-II using a Leica DMLP microscope equipped with a Linkam TMS-9 cooling-heating stage. Synthetic fluid inclusions with the triple point (–56.6 °C) of CO_2 and the melting point (0 °C), and the critical point of pure H_2O (+374.1 °C) were used to calibrate the stage. Salinities of Central European Jurassic ore-forming fluids were reported to be of the $NaCl$-$CaCl_2$-H_2O type (e.g., Behr and Gerler 1987). For sellaite formation, this system has to be expanded by Mg (to form sellaite), which renders a precise calculation of the cation composition impossible. We therefore express the salinity in mass% NaCl plus $CaCl_2$ as defined by Steele-MacInnis et al. (2011) and compare the results with other fluid inclusion data from the Clara mine by using the ice and hydrohalite melting temperatures (Fig. 3a). Pressure corrections were applied for a sedimentary cover of about 950 m during the Middle Jurassic [Rupf and Nitsch (2008): average density of 2750 kg/m^3], resulting in about 10 MPa (hydrostatic fluid pressure) to about 25 MPa (lithostatic fluid pressure), giving a 4 to 10 °C higher temperature. Analytical results are reported in Table 2.

Thermodynamic approach

To explore different variables like temperature, pressure, and activities of various chemical components in the fluid, stability calculations were performed with the HCh software package (Shvarov and Bastrakov 1999). The thermodynamic data for minerals are from Holland and Powell (1998) and from Robie and Hemingway (1995) and data for aqueous species were taken from the SUPCRT92 database and respective updates (Johnson et al. 1992; Shock et al. 1997; Sverjensky et al. 1997). All calculations of individual activity coefficients for aqueous species were applied an extended Debye-Hückel model using the b-gamma equation for NaCl as the background electrolyte (Oelkers and Helgeson 1990; Shock et al. 1992). The thermodynamic data of the minerals used are reported in Table 3 and the rock-buffered fluid conditions are reported in Table 4.

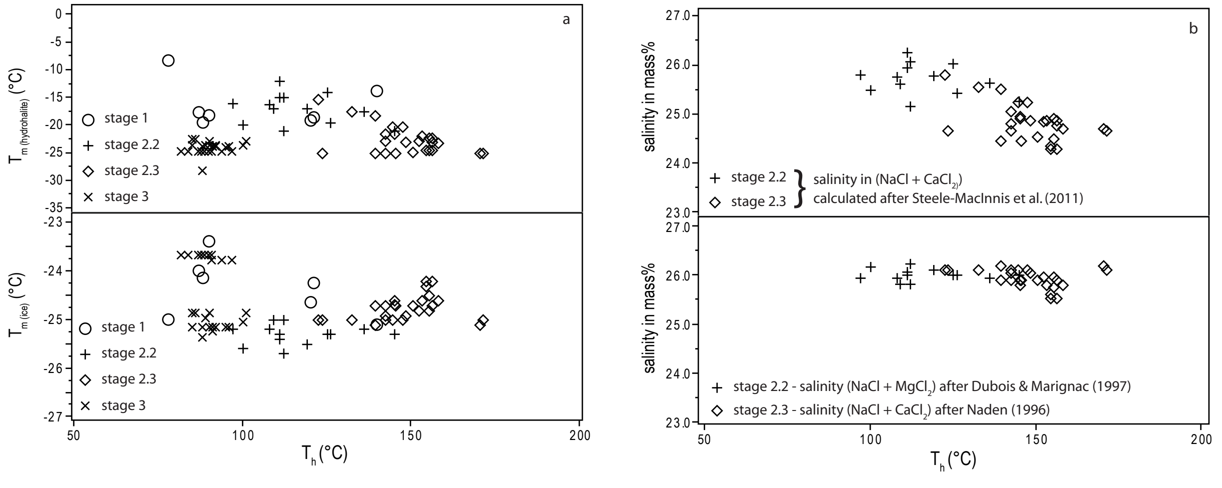

FIGURE 3. Results of stage 2.2 and 2.3 fluid inclusion investigations of sellaite and fluorite compared with data from stages 1 and 3 of the Clara vein system. (**a**): ice melting temperatures (lower box) and the hydrohalite melting temperatures (upper box) vs. the homogenization temperature and (**b**): salinities of stage 2.2 and 2.3 fluorite and sellaite. In the upper box, salinities are calculated according to Steele-MacInnis et al. (2011) and in the lower box, salinities of stage 2.2 minerals are calculated using Equations of Dubois and Marignac (1997; H_2O-$NaCl$-$MgCl_2$ system) and salinities of stage (2.3) minerals are calculated using equations of Naden (1996; H_2O-$NaCl$-$CaCl_2$ system). See text for further explanation.

TABLE 2. Fluid inclusion data of quartz, fluorite, and sellaite from the Clara mine

Stage	Mineral	$T_m$ice	$T_m$hh	T_h	mass% NaCl + $CaCl_2$	mass% NaCl	mass% $CaCl_2$	mass% NaCl+$MgCl_3$	mass% NaCl+$CaCl_2$
					Steele-MacInnis et al. (2011)			Dubois and Marignac (1997)	Naden (1996)
stage 1	quartz	–23.4	–18.3	90	24.9	18.4	6.5		
		–24.0	–17.7	87	25.2	17.2	8.0		
		–25.1	–13.8	140	26.0	15.8	10.2		
		–25.0	–8.3	78	26.5	16.6	9.9		
		–24.2	–18.6	121	25.1	16.6	8.5		
		–24.6	–19.2	120	25.2	15.8	9.5		
		–24.1	–19.5	88	25.0	16.6	8.3		
stage 2.2	fluorite	–25.0	–21.0	112	25.2	14.9	10.3	25.8	
		–25.4	–12.0	111	26.3	15.5	10.8	26.1	
		–25.6	–20.0	100	25.5	14.1	11.4	26.2	
stage 2.2	sellaite	–25.5	–17.0	119	25.8	14.7	11.1	26.1	
		–25.7	–15.0	112	26.1	14.6	11.4	26.2	
		–25.3	–15.0	111	25.9	15.3	10.7	26.0	
		–25.3	–14.0	125	26.0	15.4	10.6	26.0	
		–25.2	–17.5	136	25.6	15.1	10.6	25.9	
		–25.2	–16.0	97	25.8	15.3	10.5	25.9	
		–25.3	–19.6	126	25.4	14.6	10.8	26.0	
		–25.3	–21.0	145	25.3	14.4	10.9	26.0	
		–25.0	–17.0	109	25.6	15.5	10.1	25.8	
		–25.2	–16.3	108	25.8	15.2	10.5	25.9	
stage 2.3	fluorite	–24.7	–21.6	145	25.0	15.3	9.7		25.9
		–24.6	–21.6	145	24.9	15.5	9.4		25.8
		–24.6	–21.9	153	24.9	15.4	9.4		25.8
		–24.6	–23.3	158	24.7	15.2	9.5		25.8
		–24.9	–23.1	148	24.9	14.7	10.2		26.0
		–24.7	–25.1	139	24.5	13.9	10.5		25.9
		–24.8	–22.3	155	24.9	15.0	9.9		26.0
		–25.1	–25.0	170	24.7	14.1	10.6		26.2
		–25.0	–25.0	171	24.7	14.2	10.4		26.1
		–24.8	–22.8	152	24.9	14.9	9.9		26.0
		–24.7	–25.1	145	24.5	13.9	10.5		25.9
		–24.7	–24.8	150	24.5	14.6	10.0		25.9
		–25.0	–17.6	132	25.6	15.4	10.2		26.1
		–25.0	–25.0	123	24.7	14.2	10.4		26.1
		–24.9	–21.6	142	25.0	14.9	10.1		26.0
		–25.0	–20.3	147	25.2	15.0	10.3		26.1
		–24.7	–22.4	156	24.9	15.2	9.7		25.9
		–24.5	–24.5	155	24.5	15.2	9.3		25.8
		–24.7	–23.1	156	24.8	15.0	9.7		25.9
		–25.0	–15.3	122	25.8	15.7	10.1		26.1

TABLE 3. Thermodynamic input data and respective references

Species	$\Delta G^\circ_{f,298}$ (kJ/mol)	$\Delta S^\circ_{f,298}$ (J/mol·K)	Molar volume (cm^3)	Reference
Sellaite	−1071.10	57.20	19.610	Robie and Hemingway (1995)
Fluorite	−1175.30	68.90	24.540	Robie and Hemingway (1995)
Calcite	−1128.81	92.50	36.890	Holland and Powell (1998)
Anhydrite	−1321.80	107.40	46.010	Robie and Hemingway (1995)

RESULTS

Fluid inclusion analyses

Fluid inclusions in stage 2.2 sellaite and fluorite-II of sample SC18 from the eighth mine level were analyzed to specify the sellaite formation conditions compared to other stages of the Clara vein system (Fig. 3a).

Fluid inclusions in sellaite are difficult to identify, as the refraction indices of sellaite and the fluid are similar. However, the inclusions are rounded with two phases (liquid and vapor), with a volume fraction of the liquid of ~0.9 at room temperature. Inclusions are isolated in the center of the needles and are mostly elongated along the *c*-axis direction of the sellaite needles. Therefore, they are interpreted to be of primary origin. Fluid inclusions in fluorite-II occur as isolated inclusions. They may be of primary character and consist of two phases (liquid and vapor), with a volume fraction of the liquid of ~0.95 at room temperature. Ice melting temperatures vary from –25.7 to –25.0 °C, hydrohalite melting temperatures are –21 and –14 °C (Table 2), and homogenization temperatures in the liquid phase are between 97 and 145 °C. The salinity ranges between 25.7 and 26.0 mass% NaCl plus $CaCl_2$ [calculated using Equations of Steele-MacInnis et al. (2011); Table 2]. The occurrence of $MgCl_2 \cdot 12H_2O$ that has its melting point at approximately –37 °C (Davis et al. 1990) could not be verified as too many solid phases were still present in the inclusions at this temperature. However, these results show that fluorite and sellaite of stage 2.2 contain fluid inclusions indistinguishable from fluid inclusions of typical Jurassic fluids in the Schwarzwald ore district (Baatartsogt et al. 2007). Nonetheless, stage 2.2 fluid inclusions show slightly higher hydrohalite and slightly lower ice melting temperatures than fluid inclusions from stage 2.3 of the Clara vein (Fig. 3a; Table 2). Homogenization temperatures lie within the range of all other fluid inclusions from the Clara mine and the Schwarzwald ore district (Baatartsogt et al. 2007).

Thermodynamic approach

Sellaite has a broad stability field in *P*-*T* space as it occurs in low- (evaporite) to high-temperature environments (skarn), as well as under low- (evaporite) and high-pressure (metamorphic) conditions (Table 1). In Figure 4, the solubility of fluorite, sellaite, calcite, and anhydrite as a function of temperature and

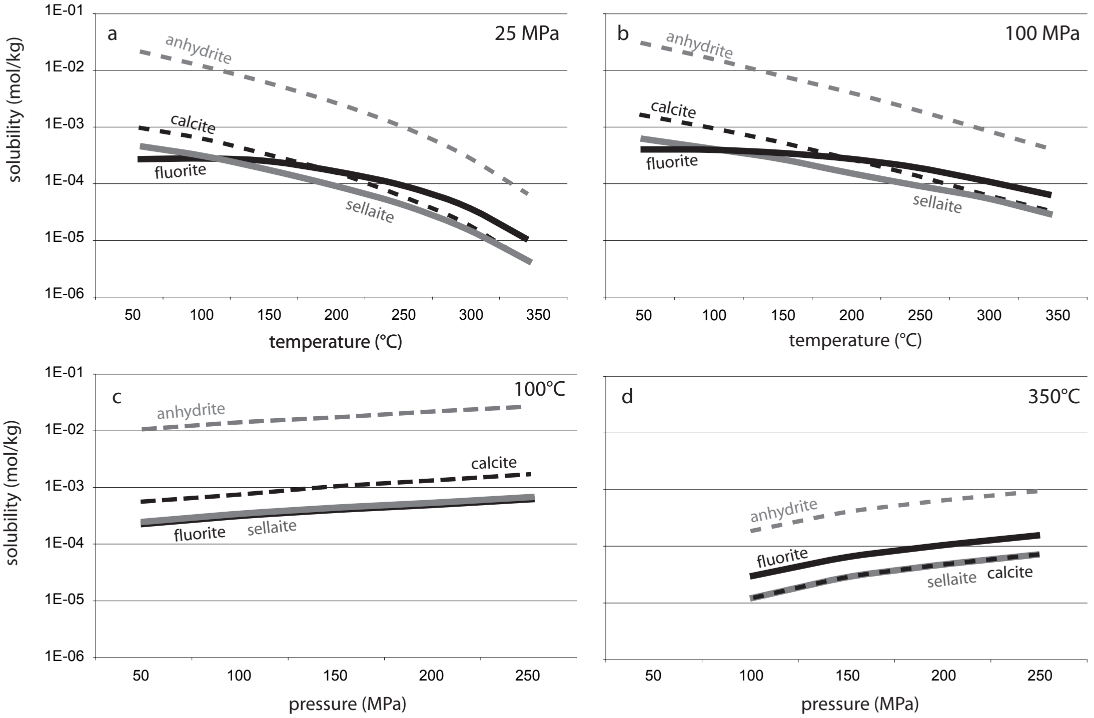

FIGURE 4. Solubilities of anhydrite, calcite, fluorite, and sellaite in a fluid with 26 wt% NaCl equivalent salinity (**a**) between 50 and 350 °C at 25 MPa, (**b**) between 50 and 350 °C at 100 MPa, (**c**) between 500 and 250 MPa at 100 °C, and (**d**) between 500 and 250 MPa at 350 °C.

TABLE 4. Gneiss-buffered fluid from the Artenberg quarry (whole-rock data and sample names published in Glodny and Grauert 2009) and from the Clara mine (whole-rock data and sample names published in Patton 1984) calculated with the HCh software package (Shvarov and Bastrakov 1999) at 150 °C

	Fluid/rock-ratio 3:100					Fluid/rock-ratio 1:100				
Artenberg	STE-3a	STE-3b	STE-3d	STE-3e	STE-3f	STE-3a	STE-3b	STE-3d	STE-3e	STE-3f
pH	5.6	5.6	5.7	5.8	5.8	5.7	5.7	6.6	6.7	6.7
Eh	–0.26	–0.26	–0.27	–0.27	–0.28	–0.26	–0.27	–0.30	–0.29	–0.29
Ca/Mg	3.20E+02	3.16E+02	5.43E+02	1.39E+02	1.29E+02	4.44E+02	5.43E+02	2.22E+00	7.27E-01	7.27E-01
Ca/Na	4.01E-06	4.01E-06	4.22E-06	2.65E-06	2.33E-06	1.59E+00	1.29E+00	1.16E+01	9.17E+00	9.17E+00
K/Na	1.35E-03	1.30E-03	2.37E-03	3.89E-04	3.23E-04	3.64E-03	5.86E-03	4.38E-03	4.53E-03	4.53E-03
Mg/Na	8.00E-03	8.20E-03	5.86E-03	1.50E-02	1.57E-02	3.59E-03	2.37E-03	5.22E+00	1.26E+01	1.26E+01
Fe/Na	4.32E-01	4.12E-01	1.29E+00	5.42E-02	4.16E-02	6.50E-06	4.22E-06	8.09E-04	1.42E-03	1.42E-03

Clara mine	Paragneiss 1	Paragneiss 20	Paragneiss 28	Orthogneiss 39A	Paragneiss 1	Paragneiss 20	Paragneiss 28	Orthogneiss 39A
pH	5.6	6.2	6.0	6.1	5.6	6.0	6.6	5.7
Eh	–0.26	–0.40	–0.41	–0.30	–0.26	–0.38	–0.40	–0.27
Ca/Mg	4.43E+02	3.46E+00	1.01E+02	9.42E+00	4.44E+02	3.43E+00	1.92E+00	9.42E+00
Ca/Na	6.73E-06	2.02E-07	1.25E-06	1.65E-06	6.79E-06	3.64E-07	5.93E-03	3.11E-06
K/Na	3.75E-03	8.12E-05	1.53E-04	1.37E-04	3.74E-03	1.41E-04	5.88E+00	4.11E-04
Mg/Na	3.63E-03	1.85E-02	1.79E-02	2.02E-02	3.65E-03	1.79E-02	4.38E-03	1.58E-02
Fe/Na	1.66E+00	2.81E-04	1.54E-02	1.29E-03	1.66E+00	4.85E-04	1.13E+01	3.87E-03

Notes: Fluid/rock-ratios are 3:100 and 1:100, respectively. Element ratios are calculated from moles.

pressure is shown. All four minerals are less soluble under higher temperature (350 °C) and lower pressure (21 MPa) conditions (Fig. 4). The exact curve progression characteristics/shape, however, varies. Assuming the same activity for Ca^{2+} and Mg^{2+} in the fluid, the reaction

$$\text{fluorite} + Mg^{2+} = \text{sellaite} + Ca^{2+}$$

is in equilibrium at 105 °C and 25 MPa, where fluorite is the stable phase below and sellaite above this temperature. However, changing Ca/Mg-ratios can influence the stability of fluorite and sellaite significantly. In Figure 5, the Ca/Mg-ratios (calculated in moles) as a function of the coexistence of fluorite and sellaite are shown as a function of temperature. This is consistent with the above-mentioned observation, i.e., at higher temperatures, Ca/Mg-ratios above unity are necessary to stabilize fluorite. Fluid inclusion analyses show temperatures between 110 and 155 °C. At these temperatures, Ca/Mg-ratios of 1.0 to 2.2 in the mineralizing fluid are necessary for the coexistence of sellaite and fluorite. Additionally, in Figure 5, rock-buffered fluids in equilibrium with different host-rock types with different fluid-rock ratios at different temperatures are reported (whole-rock data and sample names: Artenberg: Glodny and Grauert 2009; Clara mine: Patton 1984). This figure shows that the Ca/Mg-ratio of the fluid is highly dependent on the earlier alteration grade of the rock (compare work from Glodny and Grauert 2009 and from Patton 1984, i.e., pre-dating the hydrothermal event that formed the sellaite), the fluid/rock ratio, and the temperature.

DISCUSSION

It is evident from the mineral's formula (MgF_2) that the formation of sellaite instead of, or in coexistence with, fluorite requires low-Ca/Mg-ratios in the mineralizing fluid. This is easily explained for occurrences where sellaite forms in Mg-rich host-rocks (e.g., Brumado in Brazil, magnesite-rich rocks; Cassedanne and Resende 1983). However, Mg-rich host rocks are lacking at the Clara vein system and the Permian dolomite-rich calcrete horizon (which has a Ca/Mg ratio of 1) that is prevalent elsewhere in the Schwarzwald is not present in the Clara mine vicinity. Therefore, the Mg-enrichment cannot be independently explained by anomalous host rock compositions, but instead must be related to the evolution of the mineralizing fluid. In the following, we will explore: (1) the primary Mg-enrichment of the mineralizing fluid; (2) the structural control on sellaite precipitation, which appears to be confined to stage 2.2; and (3) the precipitation mechanism.

(1) Primary Mg-enrichment of the mineralizing fluid. The fluid responsible for all Jurassic mineral deposits in the Schwarzwald ore district is H_2O-NaCl-$CaCl_2$ rich, is highly saline with salinities between 20 and 28 wt% NaCl equivalent, and has homogenization temperatures between 50 and 150 °C (Baatartsogt et al. 2007). Fluids that formed stage 2.2 fluorite in the Clara vein system have the same general characteristics as stage 2.3 fluorite fluids (Figs. 3a and 3b; Table 2) and all other Jurassic mineralized occurrences, but the stage 2.2 fluorite vein is the only occurrence of sellaite in the Schwarzwald ore district. The main differences between stage 2.2 and 2.3 fluids are lower hydrohalite (stage 2.2 ranges between –21.6 and –14.0 °C and stage 2.3 ranges between –25.0 and 15.3 °C) and slightly higher ice melting temperatures in the former (stage 2.2 ranges between –25.7 and 25.0 °C and stage 2.3 ranges between –25.1 and –24.2 °C). When calculating the salinity using method by Steele-MacInnis (2011), stage 2.2 fluid inclusions have slightly higher salinities than stage 2.3 fluid inclusions (stage 2.2 salinities of >25 mass% NaCl+$CaCl_2$, and stage 2.3 mostly less than 25 mass% NaCl+$CaCl_2$). This apparent variation in salinity, however, can be caused by the prevalence

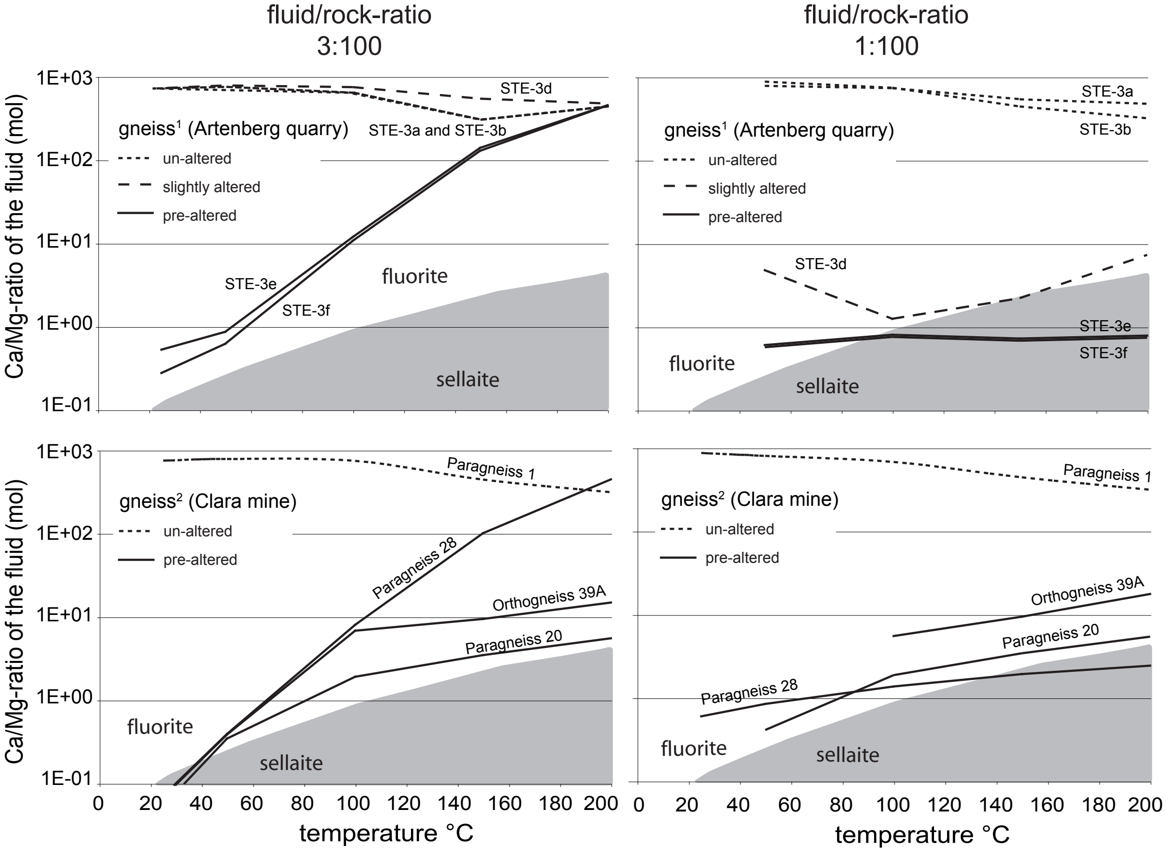

FIGURE 5. Diagram of temperature vs. Ca/Mg ratio (mole) of fluids indicating whether fluorite or sellaite is the stable phase. Fluids buffered by gneisses of different degrees of pre-alteration at 25 MPa and 150 °C were calculated with the HCh software package (Shvarov and Bastrakov 1999, Table 4). (**a**) Fluids buffered by gneisses from the Artenberg quarry (whole-rock data and sample names from Glodny and Grauert 2009) and (**b**) fluids buffered by para- and orthogneisses from the Clara mine (whole-rock data and sample names from Patton 1984) with different fluid rock ratios.

in the fluid of $MgCl_2$ compared to $CaCl_2$. For example, if stage 2.2 fluid inclusion salinities are recalculated according to the H_2O-NaCl-$MgCl_2$ system (after Dubois and Marignac 1997) and stage 2.3 fluids are calculated according to the H_2O-NaCl-$CaCl_2$ system (after Naden 1996), both stages show the same salinity of 25.9 ± 0.4 mass%.

Typical gneiss-buffered fluids in the Schwarzwald crystallize fluorite and not sellaite. Hence, the fluid's Ca/Mg ratio of the Clara fluorite vein must have been close to or below the Ca/Mg ratio indicated in Figure 4 to stabilize sellaite. Calculations show that this can only be achieved when the mineralizing fluid is in equilibrium with pre-altered gneisses (Fig. 5). The first alteration step leads to the breakdown of unstable minerals such as Ca-rich feldspar, and formation of alteration-resistant chlorite. This, in turn, leads to the passive enrichment of Mg compared to Ca in the altered rock (see also Glodny and Grauert 2009) and therefore, to lower Ca/Mg-ratios in a rock-buffered fluid, which equilibrates subsequently with this rock (Fig. 5). Moreover, Bucher et al. (2009) state that elevated Mg contents in the gneiss-buffered fluids in the Clara mine correlate with elevated K contents indicating biotite alteration.

The fluid/rock ratio also has a significant influence on Ca/Mg-ratios in the rock-buffered fluid: the smaller the ratio the more likely the fluid is capable of crystallizing sellaite instead of fluorite (Fig. 5). For the construction of Figures 5a and 5b, published whole-rock analyses (Table 4) of well-investigated unaltered and before fluid invasion gneisses from the Artenberg quarry (ca. 8 km SW of the Clara mine; Glodny and Grauert 2009) were thermodynamically equilibrated with saline fluids. The same was performed with host rocks of the Clara mine (Figs. 5c and 5d; Patton 1984). It is obvious that the higher the pre-alteration grade, the higher the temperature of the fluid and given a low-fluid/rock-ratio under disequilibrium conditions, the fluid is more likely to crystallize sellaite instead of fluorite. Field observations support these conclusions because the areas with the most intense sellaite mineralization coincide with highly pre-altered gneiss (Figs. 1 and 6a; Gerler 1987).

(2) Structural control on sellaite precipitation. Surface and underground mapping in the Clara mine (Gerler 1983; Fig. 1b) has revealed that the sellaite-bearing fluorite vein (substage 2.2 of Huck 1984) splits into several small fissures and bends below the basement-cover unconformity (forming a stockwork-like deposit), whereas all other stages are steeply dipping veins crosscutting the unconformity. Therefore, during stage 2 mineralization, the overlying sediments seal the vein-forming site and sedimentary formation waters cannot enter the depositional site (Fig. 6b). This change from open-system to a sealed-system and back to an open-system is evident from Sr-isotope systematics in barite and fluorite (Mertz 1987). Substage 2.2 is characterized by homogeneous Sr-isotopic values (0.7138 to 0.7143) indicating dominantly basement-derived Sr (Staude et al. 2011), whereas barite of stage 1 and the following substage 2.3 show more variable values between 0.7128 and 0.7153, indicating mixing of several Sr sources [e.g., basement-derived and sedimentary formation waters (Staude et al. 2011)]. This observation combined with field observations allows the interpretation that sellaite formation during substage 2.2 occurred in a sealed system controlled by the stockwork-like fissures below the basement-

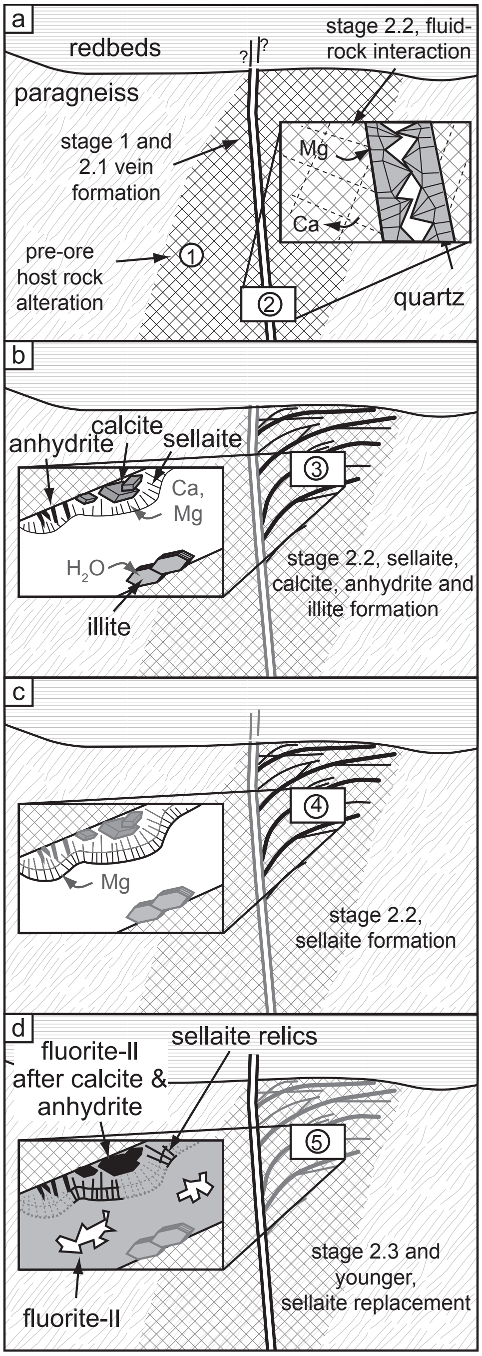

FIGURE 6. Model of sellaite formation in the Clara deposit, Oberwolfach, Schwarzwald. (**a**) Alteration of the host rock (1) observed by Gerler (1987) and formation of the mineralization stages 1 and 2.1 after Huck (1984), (2) shows fluid-rock interaction and lowering of the Ca/Mg-ratio in the mineralizing fluid. (**b**) Stockwork formation in stage 2.2, where the rock-buffered low-Ca fluid stagnates and anhydrite, calcite and illite form due to fluid-fluid and fluid-rock interaction. (**c**) Sellaite and later sellaite and fluorite formation in stage 2.2 (Huck 1984) due to fluid cooling and fluid consumption. (**d**) Sellaite is partly replaced by fluorite-II in a younger stage. In stage 2.3, the depositional site is not sealed by overlaying sediments anymore. See text for explanation.

cover unconformity with only minor involvement of sedimentary formation waters. Based on our knowledge from the literature, the bending below the unconformity is a unique feature in the Schwarzwald ore district, and it may have served to retard the repeated upward fluid flow within the network, increase the reaction and ultimately in mineral precipitation (Fig. 6c).

(3) Precipitation mechanisms. The dominant mechanisms of precipitation for hydrothermal deposits in the Schwarzwald ore district are fluid cooling and fluid mixing (Behr and Gerler 1987; Schwinn et al. 2006; Baatartsogt et al. 2007; Pfaff et al. 2010, 2011; Staude et al. 2009, 2010a, 2011, 2012). Fluid mixing as the driving force for sellaite precipitation can be ruled out, as all fluids involved most likely have the same overall gneiss-buffered geochemistry. Changes in pH and oxygen fugacity [the hot ascending fluid had a lower pH and was more oxidized compared to the gneiss-buffered formation waters at the depositional site (see Pfaff et al. 2010)] have no impact on sellaite precipitation. However, mixing of hot ascending brines with gneiss-buffered formation waters in the stockwork fissures may have precipiated carbonates and anhydrite due to changes in pH (increase in pH) and thereby lowered the Ca/Mg-ratio of the already Ca-depleted gneiss-buffered fluid. As the fluid stagnated within the fissure, fluid cooling (Fig. 7a) and fluid consumption (Fig. 7b) may have played important roles. Fluid cooling favors fluorite precipitation. However, fluid inclusion studies suggest that sellaite precipitation started at higher temperatures and was followed by fluorite precipitation that replaced earlier sellaite (Fig. 7a). The stagnating fluid also reacted with the host rock and caused the formation of illite (see Brockamp and Clauer 2005). These illite crystals also occur as inclusions in fluorite of this mineralization stage (Fig. 2d). During illite formation, water was consumed and depleted the fluid in water ("desiccation," e.g., Markl and Bucher 1998), resulting in over-saturation of the remaining fluid first with respect to sellaite, followed by fluorite (Figs. 2g and 7b). Therefore, fluid consumption, which is enhanced by decreasing temperatures, was probably another precipitation mechanism for sellaite in the Clara vein system (Fig. 7b), although temperature decrease was certainly more important (compare Figs. 7a and 7b). Subsequently, during a younger event, the stockwork-like vein system (compare Fig. 1) was tectonically not active any more resulting in a "normal" increased Ca/Mg-ratio, in fluorite-II precipitation and in sellaite replacement. Possibly, due to changing pH conditions and dilution, the carbonates and anhydrite crystals grown prior or parallel to the sellaite formation were dissolved and also replaced by fluorite-II (Fig. 6d).

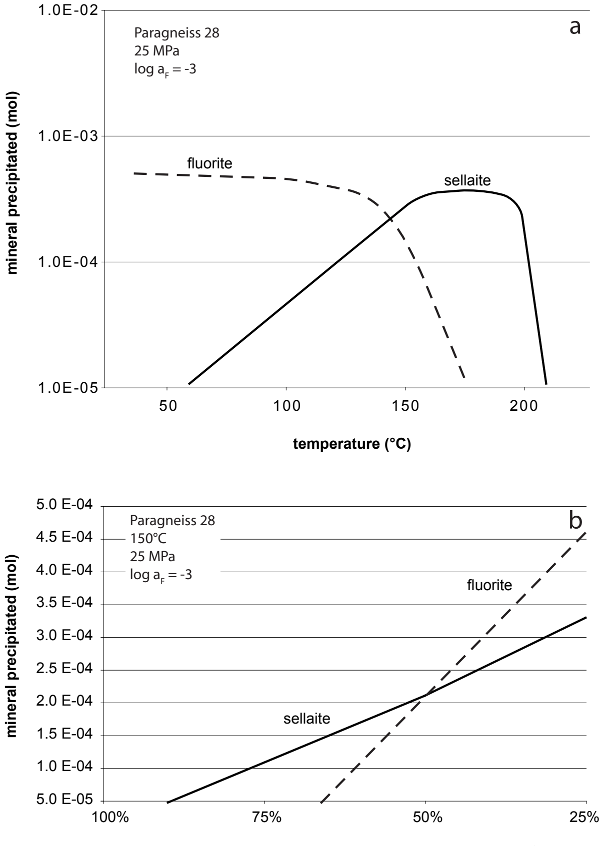

FIGURE 7. Rock-buffered fluid (fluid/rock-ratio of 1:100) from Figure 5 and Table 4 (paragneiss 28: Patton 1984) as a function of fluid cooling (**a**) and with decreasing H_2O-content simulating fluid consumption during illite precipitation and fluid-rock interaction at 150 °C (**b**). Sellaite starts to precipitate at higher temperatures compared to fluorite, is cogenetic with fluorite at around 150 °C and is replaced by fluorite below 150 °C. Moreover, sellaite precipitation occurs when about 10% of the original fluid is consumed, while fluorite co-precipitates only, after around 35% of the fluid is consumed.

ACKNOWLEDGMENTS

We gratefully acknowledge the discussions with Thomas Wenzel, the help with the Chinese literature of Lianxun Wang (Tübingen, Germany), and the help with literature search of Ryan Taylor (USGS, Denver, U.S.A.) and Ulrike van Raden (ETH Zurich). The research of this publication was supported by the Alfried Krupp Prize for Young University Teachers of the Krupp Foundation to Gregor Markl. Moreover, we greatly acknowledge the very helpful and constructive reviews of Karen Kelley and Michel Dubois.

REFERENCES CITED

Baatartsogt, B., Schwinn, G., Wagner, T., Taubald, H., Beitter, T., and Markl, G. (2007) Contrasting paleofluids system in the continental basement: A fluid inclusion and stable isotope study of hydrothermal vein mineralization, Schwarzwald district, Germany. Geofluids, 7, 123–147.

Behr, H.J. and Gerler, J. (1987) Inclusions of sedimentary brines in post-Variscan mineralizations in the Federal Republic of Germany: A study by Neutron Activation Analysis. Chemical Geology, 61, 65–77.

Brockamp, O. and Clauer, N. (2005) A km-scale illite alteration zone in sedimentary wall rocks adjacent to a hydrothermal fluorite vein deposit. Clay Minerals, 40, 245–260.

Bucher, K., Zhu, Y., and Stober, I. (2009) Groundwater in fractured crystalline rocks, the Clara mine, Black Forest (Germany). International Journal of Earth Sciences, 98, 1727–1739.

Cassadenne, J.P. and Resende, J.P. (1983) Sellaite from the Brumado mine. The Mineralogical Record, 14, 179–181.

Davis, D.W., Lowenstein, T.K., and Spencer, R.J. (1990) Melting behaviour of fluid inclusions in laboratory-grown halite crystals in the systems NaCl-H_2O, NaCl-KCl-H_2O, NaCl-$MgCl_2$-H_2O, and NaCl-$CaCl_2$-H_2O. Geochimica et Cosmochimica Acta, 54, 591–601.

Dubois, M. and Marignac, C. (1997) The H_2O-NaCl-$MgCl_2$ ternary phase diagram with special application to fluid inclusion studies. Economic Geology, 92, 114–119.

Ellmies, R., Krupenin, M.T., Germann, K., Möller, P., and Echtler, H.P. (1999) The fluorite-sellaite deposits of Suran (Bashkir Meganticline, Urals). Processes to Processing, 841–844.

Franzke, H.J., Werner, W., and Wetzel, H.U. (2003) Die Anwendung von Satellitenbilddaten zur tektonischen Analyse des Schwarzwalds und des angrenzenden Oberrheingrabens. Jahreshefte des Geologischen Landesamt Baden-Württemberg, 39, 25–54.

Gerler, J. (1983) Geologische Kartierung in der Umgebung der Lagerstätte "Clara" bei Oberwolfach (Mittlerer Schwarzwald). Unpublished diploma mapping, University of Göttingen.

——— (1987) Spurenelemente in Hydrothermalquarzen und deren Beziehung zur Masse und Salinität von Flüssigkeitseinschlüssen. Beiheft 1 zu Fortschritte der Mineralogie, 65, 56.

Glodny, J. and Grauert, B. (2009) Evolution of a hydrothermal fluid-rock interaction system as recorded by Sr isotopes: A case study from the Schwarzwald, SW Germany. Mineraloy and Petrology, 95, 163–178.

Grice, J.D., Gault, R.A., and Van Velthuizen, J. (1996) Penobsquisite: A new borate mineral with a complex framework structure. Canadian Mineralogist, 34, 657–665.

——— (2005) Borate minerals of the Penobsquis and Millstream deposits, southern New Brunswick, Canada. Canadian Mineralogist, 43, 1469–1487.

Halley, S.W. and Walshe, J.L. (1995) A Reexamination of the Mount Bischoff cassiterite sulfide skarn, western Tasmania. Economic Geology, 90, 1676–1693.

Harris, J.W. (1969) The recognition of diamond inclusions-Pt 2: Epigenetic mineral inclusions. Industrial Diamond Review, 28, 458–461.

Hofmann, A. and Köhler, H. (1973) Whole rock Rb-Sr ages of anatectic gneisses from the Schwarzwald, SW Germany. Neues Jahrbuch für Geologie und Paläontologie, Abhandlungen, 119, 163–187.

Holland, T.J.B. and Powell, R. (1998) An internally consistent thermodynamic data set for phases of petrological interest. Journal of Metamorphic Geology, 16, 309–343.

Huck, K.H. (1984) Die Beziehung zwischen Tektonik und Paragenese unter Berücksichtigung geochemischer Kriterien in der Fluß- und Schwerspatlagerstätte “Clara” bei Oberwolfach/Schwarzwald. Dissertation, University of Heidelberg.

Imai, H., Kawasaki, M., Yamaguchi, M., and Takahashi, M. (1985) Mineralization and paragenesis of the Huanzala mine, central Peru. Economic Geology, 80, 461–478.

Johnson, J.W., Oelkers, E.H., and Helgeson, H.C. (1992) Supcrt92: a software package for calculating the standard molal thermodynamic properties of minerals, gases, aqueous species, and reactions from 1 to 5000 bars and 0 to 1000 C. Computational Geosciences, 18, 899–947.

Kalt, A., Altherr, R., and Hanel, M. (2000) The Variscan basement of the Schwarzwald. Beihefte zum European Journal of Mineralogy, 12, 1–43.

Keller, J. and Krafft, M. (1990) Effusive natrocarbonatite activity of Oldoinyo Lengai, June 1988. Bulletin of Volcanology, 52, 629–645.

Kühn, R. (1951) Sellaite als salinares Mineral. Fortschritte der Mineralogie, 30, 390.

Lottermoser, B.G. and Lu, J. (1997) Petrogenesis of rare-element pegmatites in the Olary Block, South Australia, part 1. Mineralogy and chemical evolution. Mineralogy and Petrology, 59, 1–19.

Maag, W. (1987) Hydrothermale Stoffzufuhr in Sedimenten des Buntsandsteins im Bereich der Fluß- und Schwerspatlagerstätte “Clara” (mittlerer Schwarzwald). Unpublished diploma thesis, University of Heidelberg.

Markl, G. and Bucher, K. (1998) Composition of fluids in the lower crust inferred from metamorphic salt in lower crustal rocks. Nature, 391, 781–783.

Markl, G., von Blanckenburg, F., and Wagner, T. (2006a) Iron isotope fractionation during hydrothermal ore deposition and alteration. Geochimica et Cosmochimica Acta, 70, 3011–3030.

Markl, G., Lahaye, Y., and Schwinn, G. (2006b) Copper isotopes as monitors of redox processes in hydrothermal mineralization. Geochimica et Cosmochimica Acta, 70, 4215–4228.

Matter, A., Peters, T., and Ramseyer, K. (1987) ^{87}Sr/^{86}Sr-Verhältnisse und Sr-Gehalte von Tiefengrundwässern, Mineralien sowie aus dem Krisallin und der Trias der Nordschweiz. Eclogae Geologicae Helvetiae, 80, 579–592.

Maus, H.J. (1977) Violetter Fluorit und Sellait von der Grube Clara, Oberwolfach, Schwarzwald. Aufschluss, 28, 361–367.

Maus, H.J., Gundlach, H., and Podufal, P. (1979) Über den Sellait (MgF_2) der Grube Clara, Oberwolfach, Mittlerer Schwarzwald. Neues Jahrbuch für Mineralogie, Abhandlungen, 136, 10–25.

Mertz, D.F. (1987) Isotopengeochemische und mineralogische Untersuchungen an postvariscischen hydrothermalen Silikaten. Dissertation, University of Heidelberg.

Mertz, D.F., Lippolt, H.J., and Huck, K.H. (1986) K/Ar, Ar-40/Ar-39, and Rb/Sr investigations on the genesis of the Clara vein deposit, Central Black Forest. Jahrestagung der Deutschen Geophysikalischen Gesellschaft eV, 46, 235.

Mitchell, R.H. (1997) Carbonate-carbonate immiscibility, neighborite and potassium iron sulphide in Oldoinyo Lengai natrocarbonatite. Mineralogical Magazine, 61, 779–789.

Naden, J. (1996) CalcicBrine: A Microsoft Excel 5.0 add-in for calculating salinities from microthermometric data in the system $NaCl-CaCl_2-H_2O$. In P.E. Brown and S.G. Hagemann, Eds., PACROFI VI. Madison, Wisconsin.

Oelkers, E.H. and Helgeson, H.C. (1990) Triple-ion anions and polynuclear complexing in supercritical electrolyte solutions. Geochimica et Cosmochimica Acta, 54, 727–738.

Patton, J.F. (1984) Hydrothermale Umwandlungen am Nebengestein der Schwerspat- und Flussspatgänge der Grube “Clara” (mittlerer Schwarzwald) und ihre Bedeutung für die Genese der Lagerstätten. Diploma thesis, University of Freiburg i Brsg.

Pfaff, K., Romer, R.L., and Markl, G. (2009) U-Pb ages of ferberite, chalcedony, agate, “U-mica” and pitchblende: Constraints on the mineralization history of the Schwarzwald ore district. European Journal of Mineralogy, 21, 817–836.

Pfaff, K., Hildebrandt, L.H., Leach, D.L., Jacob, D.E., and Markl, G. (2010) Formation of the Mississippi Valley-Type Zn-Pb-Ag deposit in the extensional setting of the Upper Rhinegraben in the Wiesloch area, SW Germany. Mineralium Deposita, 45, 647–666.

Pfaff, K., Koenig, A., Wenzel, T., Ridley, I., Hildebrandt, L.H., Leach, D.L., and Markl, G. (2011) Trace and minor element variations and sulfur isotopes in crystalline and colloform ZnS: Incorporation mechanisms and implications for their genesis. Chemical Geology, 286, 118–134.

Robie, R.A. and Hemingway, B.S. (1995) Thermodynamic properties of minerals and related substances at 198.15 K and 1 bar (10^5 Pascals) pressure and at higher temperatures. U.S. Geological Survey, Bulletin 2131, 461 p.

Röper, H.P. (1980) Zur Petrographie und Genese des Karneoldolomit-Horizontes im Gebiet des mittleren Schwarzwaldes. Dissertation, University of Heidelberg.

Rupf, I. and Nitsch, E. (2008) Das geologische Landesmodell von Baden-Württemberg: Datengrundlagen, technische Umsetzung und erste geologische Ergebnisse. LGRB Informationen, 21, 1–82.

Schleicher, H. (1994) Collision-type granitic melts in the context of the thrust tectonics and uplift history (Triberg Granite Complex, Schwarzwald, Germany). Neues Jahrbuch für Mineralogie, Abhandlungen, 166, 211–237.

Schwinn, G. and Markl, G. (2005) REE systematics in hydrothermal fluorite. Chemical Geology, 216, 225–248.

Schwinn, G., Wagner, T., Baatartsogt, B., and Markl, G. (2006) Quantification of mixing processes in ore-forming hydrothermal systems by combination of stable isotope and fluid inclusion analyses. Geochimica et Cosmochimica Acta, 770, 965–982.

Shock, E.L., Oelkers, E.H., Johnson, J.W., Sverjensky, D.A., and Helgeson, H.C. (1992) Calculation of the thermodynamic properties of aqueous species at high pressures and temperatures> effective electrostatic radii, dissociation constants and standard partial molal properties to 1000 C and 5 kbar. Journal of the Chemical Society, Faraday Transactions, 88, 803–826.

Shock, E.L., Sassani, D.C., Willis, M., and Sverjensky, D.A. (1997) Inorganic species in geological fluids: correlations among standard molal thermodynamic properties of aqueous ions and hydroxide complexes. Geochimica et Cosmochimica Acta, 61, 907–950.

Shvarov, Y.V. and Bastrakov, E. (1999) HCh: A software package for geochemical equilibrium modeling. Record 1999/25, Australian Geological Survey Organisation, Canberra, Australia.

Sokol, E.V., Nigmatulina, E.N., and Volkova, N.I. (2002) Fluorine mineralisation from burning coal spoil-heaps in the Russian Urals. Mineralogy and Petrology, 75, 23–40.

Staude, S., Wagner, T., and Markl, G. (2007) Mineralogy, mineral chemistry and fluid evolution of the hydrothermal Wenzel deposit, southern Germany: Implications for the formation of Kongsberg-type silver deposits. Canadian Mineralogist, 45, 1147–1176.

Staude, S., Bons, P.D., and Markl, G. (2009) Hydrothermal vein formation by extension-driven dewatering of the middle crust: An example from SW Germany. Earth and Planetary Science Letters, 286, 387–395.

Staude, S., Dorn, A., Pfaff, K., and Markl, G. (2010a) Assemblages of Ag-Bi sulfosalts and conditions of their formation: The type locality of schapbachite ($Ag_{0.4}Pb_{0.2}Bi_{0.4}S$) and neighboring mines in the Schwarzwald ore district, southern Germany. Canadian Mineralogist, 48, 441–466.

Staude, S., Mordhorst, T., Neumann, R., Prebeck, W., and Markl, G. (2010b) Compositional variation of the tennantite-tetrahedrite solid-solution series in the Schwarzwald ore district (SW Germany): The role of mineralizing processes and fluid source. Mineralogical Magazine, 74, 309–338.

Staude, S., Göb, S., Pfaff, K., Ströbele, F., Premo, W.R., and Markl, G. (2011) Deciphering fluid sources of hydrothermal systems: a combined Sr- and S-isotope study on barite (Schwarzwald, SW Germany). Chemical Geology, 286, 1–20.

Staude, S., Werner, W., Mordhorst, T., Wemmer, K., and Markl, G. (2012) The complex multi-stage Co-Ni-Bi-U and Cu-Bi hydrothermal mineralization at Wittichen, Schwarzwald, SW Germany: Ore mineralogy, geological setting and conditions of mineralization. Mineralium Deposita, 47, 251–276.

Steele-MacInnis, M., Bodnar, R.J., and Naden, J. (2011) Numerical model to determine the composition of $H_2O-NaCl-CaCl_2$ fluid inclusions based on microthermometric and microanalytical data. Geochimica et Cosmochimica Acta, 75, 21–40.

Sverjensky, D.A., Shock, E.L., and Helgeson, H.C. (1997) Prediction of the thermodynamic properties of aqueous metal complexes to 1000 C and 5 kb. Geochimica et Cosmochimica Acta, 61, 1359–1412.

Zambezi, P., Voncken, J.H.L., Hale, M., and Touret, J.L.R. (1997) Bastnäsite-(Ce) at the Nkombwa Hill carbonatite complex, Isoka District, northeast Zambia. Mineralogy and Petrology, 59, 239–250.

Manuscript received January 22, 2012
Manuscript accepted July 7, 2012
Manuscript handled by Hongwu Xu